Arch Appl Mech (2017) 87:87–98
DOI 10.1007/s00419-016-1178-9

ORIGINAL

Xu Wang · Peter Schiavone

Interaction between an edge dislocation and a circular inhomogeneity with a mixed-type imperfect interface

Received: 20 April 2016 / Accepted: 3 September 2016 / Published online: 13 September 2016

Abstract We present an analytical solution (in series form) to the plane strain problem associated with an edge dislocation in the vicinity of a circular elastic inhomogeneity with a 'mixed-type imperfect interface.' The latter is a representation of the interfacial region in which the inhomogeneity and the matrix are endowed with separate and distinct Gurtin–Murdoch surface elasticities and bonded together through a spring-type imperfect interface. The coefficients in the resulting series solution are determined in a rather elegant manner requiring only the inverse of a number of 4×4 real symmetric positive definite matrices. The stress distribution in the composite structure and the normalized image force acting on the edge dislocation are found to be dependent on six size-dependent dimensionless parameters, among which four arise from the associated surface elasticities and two from the linear spring model of the interface. Asymptotic expressions for the image force when the dislocation is located at a remote distance from the inhomogeneity are also obtained analytically. The correctness of the solution is verified both numerically and analytically by comparison with existing results in the literature. Most importantly, our numerical results indicate that it is possible to find multiple equilibrium positions for the edge dislocation.

Keywords Mixed-type imperfect interface · Circular inhomogeneity · Edge dislocation · Image force · Size dependency

1 Introduction

The interaction of dislocations with elastic inhomogeneities has attracted the attention of theoreticians and practitioners alike (see, for example, [3–7,12,19,23–25]). The inhomogeneity–matrix interface remains a critical focus point in the analysis of the dislocation–inhomogeneity interaction problem. In an effort to allow tractability of the ensuing mathematical models, early studies assumed an idealized model of the interface, for example, perfectly bonded [5,6] or sliding [4]. In an effort to more accurately model the influence of the interface, in particular to account for interface damage (for example, debonding, sliding and/or micro-cracking across the interface), the linear spring model has been introduced into the dislocation–inhomogeneity interaction problem [7,19,23]. This more comprehensive interface model is based on the assumption that tractions are continuous, but displacements are discontinuous across the interface. More precisely, jumps in the

X. Wang
School of Mechanical and Power Engineering, East China University of Science and Technology,
130 Meilong Road, Shanghai 200237, China
E-mail: xuwang@ecust.edu.cn

P. Schiavone (✉)
Department of Mechanical Engineering, University of Alberta, 10-203 Donadeo Innovation Centre for Engineering,
Edmonton, AB T6G 1H9, Canada
E-mail: p.schiavone@ualberta.ca

displacement components are proportional to their respective interface traction components in terms of 'spring-factor-type' interface parameters [16]. The linear spring interface model is also referred to as a 'soft interface' since it is particularly appropriate when modeling a soft and thin interphase layer lying between two elastic media [1]. It is well known that when composite assemblies involving elastic inhomogeneities are analyzed at much smaller length scales (for example, at the nanoscale), the increasing surface area-to-bulk volume ratio means that the effects of surface mechanics (on all surfaces involved in the assembly) play a significant role in the overall deformation of the composite [17]. One of the most commonly adopted 'surface models' is the continuum-based surface/interface model of Gurtin and Murdoch [9–11]. In the absence of residual surface tension, the Gurtin–Murdoch model is strictly equivalent to the membrane-type stiff interface referred to in [1, 2]. The Gurtin–Murdoch model has recently been incorporated into the study of the dislocation–inhomogeneity interaction problem [8,13,20]. Most recently, the current authors [21,22] have proposed the so-called mixed-type imperfect interface model to account for the most accurate representation of possible interface damage in nanosized inhomogeneities. In this interface model, both the inhomogeneity and the matrix are endowed with separate and distinct surface elasticities and bonded through a spring-type imperfect interface. This allows for a comprehensive account of the contribution of each of the surfaces involved in the mechanical analysis.

In this paper, the mixed-type imperfect interface is incorporated into the interaction problem of an edge dislocation near a circular elastic inhomogeneity. A simple and effective method based on analytic continuation is proposed to solve the interaction problem with highly unusual and nonstandard boundary/interface conditions. The image force acting on the edge dislocation is also derived using the analytic solution obtained and the Peach–Koehler formula [3]. The size dependency of the induced stress field and the normalized image force is clearly demonstrated. The correctness of the obtained solution is carefully verified by comparison with the classical solutions of Dundurs [3] for a perfectly bonded interface and Dundurs and Gangadharan [4] for a sliding interface.

The paper is structured as follows: In Sect. 2, the bulk elasticity, the surface elasticity and the spring-type imperfect interface models are reviewed briefly for completeness. In Sect. 3, an analytic solution to the dislocation–inhomogeneity interaction problem is subsequently derived. Explicit expressions for the image force in the case of gliding and climbing dislocations are presented in Sect. 4 as well as analytic results for the long-range interaction results when the dislocation is located remotely with respect to the inhomogeneity.

2 Formulation

2.1 The bulk elasticity

In what follows, unless otherwise stated, Latin indices i, j, k take the values 1,2,3 and we sum over repeated indices. In a Cartesian coordinate system $\{x_i\}$, the equilibrium equations and the constitutive relations describing the deformation of a linearly elastic, homogeneous and isotropic bulk solid are given by

$$\sigma_{ij,j} = 0, \sigma_{ij} = 2\mu\varepsilon_{ij} + \lambda\varepsilon_{kk}\delta_{ij}, \varepsilon_{ij} = \frac{1}{2}(u_{i,j} + u_{j,i}), \tag{1}$$

where λ and μ are Lamé constants, σ_{ij} and ε_{ij} are, respectively, the Cartesian components of the stress and strain tensors in the bulk material, u_i is the ith component of the displacement vector, and δ_{ij} is the Kronecker delta.

For plane strain problems, the stresses, displacements and associated stress functions ϕ_1, ϕ_2 can be expressed in terms of two analytic functions $\varphi(z)$ and $\psi(z)$ of the complex variable $z = x_1 + \mathrm{i}x_2$ as [14,18]

$$\begin{aligned}
\sigma_{11} + \sigma_{22} &= 2\left[\varphi'(z) + \overline{\varphi'(z)}\right], \\
\sigma_{22} - \sigma_{11} + 2\mathrm{i}\sigma_{12} &= 2\left[\bar{z}\varphi''(z) + \psi'(z)\right], \\
2\mu(u_1 + \mathrm{i}u_2) &= \kappa\varphi(z) - z\overline{\varphi'(z)} - \overline{\psi(z)}, \\
\phi_1 + \mathrm{i}\phi_2 &= \mathrm{i}\left[\varphi(z) + z\overline{\varphi'(z)} + \overline{\psi(z)}\right],
\end{aligned} \tag{2}$$

where $\kappa = 3 - 4\nu$ in which $\nu (0 \le \nu \le 1/2)$ is Poisson's ratio. In addition, the stresses are related to the stress functions through [18]

$$\begin{aligned}
\sigma_{11} &= -\phi_{1,2}, \ \sigma_{12} = \phi_{1,1}, \\
\sigma_{21} &= -\phi_{2,2}, \ \sigma_{22} = \phi_{2,1}.
\end{aligned} \tag{3}$$

Let t_1 and t_2 be traction components along the x_1- and x_2-directions, respectively, on a boundary L. If s is the arc length measured along L such that, when facing the direction of increasing s, the material remains on the left-hand side, and it can be shown that [18]

$$t_1 + \mathrm{i}t_2 = -\frac{\mathrm{d}(\phi_1 + \mathrm{i}\phi_2)}{\mathrm{d}s}. \tag{4}$$

2.2 The Gurtin–Murdoch surface elasticity

The equilibrium conditions on a surface incorporating interface/surface elasticity according to the Gurtin–Murdoch theory can be expressed as [9–11,15]:

$$\begin{aligned} &[\sigma_{\alpha j} n_j \underline{e}_\alpha] + \sigma^{\mathrm{s}}_{\alpha\beta,\beta}\underline{e}_\alpha = 0, \quad \text{(tangential direction)} \\ &[\sigma_{ij} n_i n_j] = \sigma^{s}_{\alpha\beta}\kappa_{\alpha\beta}, \quad \text{(normal direction)} \end{aligned} \tag{5}$$

where n_i is the ith component of the outward unit normal vector to the surface, $[*]$ denotes the jump across the surface, and $\sigma^{\mathrm{s}}_{\alpha\beta}$ and $\kappa_{\alpha\beta}$ are the components of the surface stress tensor and the surface curvature tensor, respectively. In addition, the constitutive equations on the isotropic surface are given by

$$\sigma^{\mathrm{s}}_{\alpha\beta} = \sigma_0\delta_{\alpha\beta} + 2(\mu_s - \sigma_0)\varepsilon^{\mathrm{s}}_{\alpha\beta} + (\lambda_s + \sigma_0)\varepsilon^{\mathrm{s}}_{\gamma\gamma}\delta_{\alpha\beta}, \tag{6}$$

where $\varepsilon^{\mathrm{s}}_{\alpha\beta}$ are the components of the surface strain tensor, σ_0 is the surface tension, and λ_s and μ_s are the two surface Lamé constants.

We mention that in Eqs. (5) and (6), the Greek indices α, β and γ take on values of the surface components. For example, in the case of circular cylindrical fibers, α, β, γ each takes on the values θ, z.

2.3 The spring-type imperfect interface

Denote by u_r and u_θ the respective components of the displacement vector, normal and tangential to the inhomogeneity–matrix interface L and σ_{rr},$\sigma_{r\theta}$ the normal and shear components, respectively, of the traction along the interface L. The interface conditions on the spring-type imperfect interface are [1].

$$[\sigma_{rr} + \mathrm{i}\sigma_{r\theta}] = 0, \sigma_{rr} = k_r[u_r], \ \sigma_{r\theta} = k_\theta[u_\theta], \quad \text{on} \quad L, \tag{7}$$

where k_r and k_θ are two nonnegative interface parameters and $[*] = [*]_M - [*]_I$ denotes the jump across L (with subscripts 'M' and 'I' denoting the matrix and inhomogeneity, respectively).

3 An edge dislocation near a circular inhomogeneity with a mixed-type imperfect interface

Consider a domain in $\Re^2$, infinite in extent, containing a single circular elastic inhomogeneity with elastic properties different from those of the surrounding matrix, as shown in Fig. 1. The inhomogeneity, with its center at the origin of the coordinate system and radius R, occupies a region denoted by S_1. The matrix occupies the region S_2, and the inhomogeneity–matrix interface is represented by the curve L. In what follows, the subscripts 1 and 2 [or the superscripts (1) and (2)] are used to identify the respective quantities in S_1 and S_2. Separate surface elasticities are simultaneously incorporated into the surface of the inhomogeneity and into that of the matrix. In addition, the two phases are bonded through a spring-type imperfect interface as described above. An edge dislocation with Burgers vector (b_1, b_2) is located at $(\xi, 0)$ on the x_1-axis in the matrix. The composite remains free from any other external loading.

If we assume that the interface L is coherent (i.e., $\varepsilon^{\mathrm{s}}_{\alpha\beta} = \varepsilon_{\alpha\beta}$) with respect to either the inhomogeneity or the matrix, it follows from Eqs. (5) and (6) that the boundary conditions on the surfaces of the circular inhomogeneity and the surrounding matrix can be written in the form

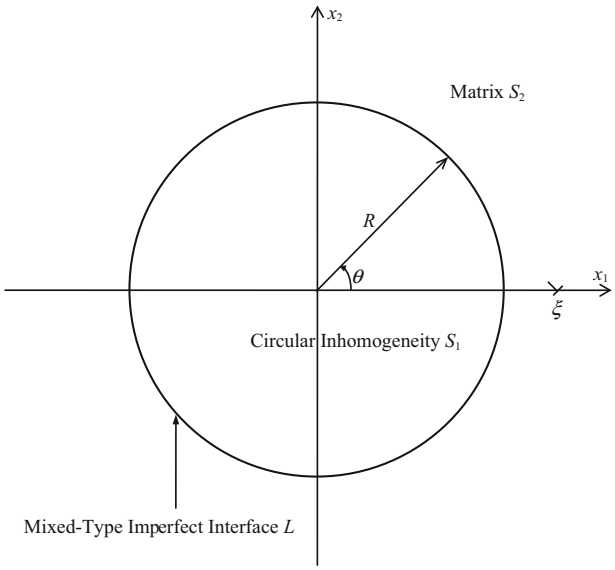

Fig. 1 An edge dislocation near a circular inhomogeneity with a mixed-type imperfect interface

$$(\sigma_{rr}^{(1)}+\mathrm{i}\sigma_{r\theta}^{(1)})-(\sigma_{rr}^{-}+\mathrm{i}\sigma_{r\theta}^{-})=-\frac{\sigma_0^{(1)}}{R}+\frac{J_0^{(1)}}{R^2}\left[\mathrm{i}\frac{\partial^2 u_\theta^{(1)}}{\partial\theta^2}+\mathrm{i}\frac{\partial(u_r^{(1)}+\mathrm{i}u_\theta^{(1)})}{\partial\theta}-u_r^{(1)}\right],$$
$$\text{on the surface of the inhomogeneity,} \tag{8}$$

$$(\sigma_{rr}^{+}+\mathrm{i}\sigma_{r\theta}^{+})-(\sigma_{rr}^{(2)}+\mathrm{i}\sigma_{r\theta}^{(2)})=-\frac{\sigma_0^{(2)}}{R}+\frac{J_0^{(2)}}{R^2}\left[\mathrm{i}\frac{\partial^2 u_\theta^{(2)}}{\partial\theta^2}+\mathrm{i}\frac{\partial(u_r^{(2)}+\mathrm{i}u_\theta^{(2)})}{\partial\theta}-u_r^{(2)}\right],$$
$$\text{on the surface of the matrix,} \tag{9}$$

where $J_0^{(j)}=2\mu_s^{(j)}+\lambda_s^{(j)}-\sigma_0^{(j)}\geq 0$, $j=1,2$, and

$$\sigma_{rr}^{-}+\mathrm{i}\sigma_{r\theta}^{-}=\sigma_{rr}^{+}+\mathrm{i}\sigma_{r\theta}^{+}=\frac{k_r+k_\theta}{2}\left[(u_r^{(2)}+\mathrm{i}u_\theta^{(2)})-(u_r^{(1)}+\mathrm{i}u_\theta^{(1)})\right]$$
$$+\frac{k_r-k_\theta}{2}\left[(u_r^{(2)}-\mathrm{i}u_\theta^{(2)})-(u_r^{(1)}-\mathrm{i}u_\theta^{(1)})\right], \tag{10}$$

According to Eq. (7), Eqs. (8)–(10) describe a mixed-type imperfect interface under inplane deformations. The imperfect interface model in Eqs. (8)–(10) contains six nonnegative imperfect interface parameters $J_0^{(1)}$, $J_0^{(2)}$, $\sigma_0^{(1)}$, $\sigma_0^{(2)}$, k_r, k_θ. In order to solve the boundary value problem, we introduce the following analytical continuations:

$$\begin{aligned}\varphi_1(z)&=-z\bar{\varphi}_1'(R^2/z)-\bar{\psi}_1(R^2/z),\quad |z|>R,\\ \varphi_2(z)&=-z\bar{\varphi}_2'(R^2/z)-\bar{\psi}_2(R^2/z),\quad |z|<R.\end{aligned} \tag{11}$$

Consequently, the boundary conditions in Eqs. (8)–(10) can be concisely expressed in terms of $\varphi_1(z)$, $\varphi_2(z)$ and their analytic continuations are as follows

$$\begin{aligned}&\varphi_1'^{+}(z)-\varphi_1'^{-}(z)-\tfrac{k_r+k_\theta}{4}\left[\tfrac{R}{\mu_2}\left(\kappa_2 z^{-1}\varphi_2^{-}(z)+z^{-1}\varphi_2^{+}(z)\right)-\tfrac{R}{\mu_1}\left(\kappa_1 z^{-1}\varphi_1^{+}(z)+z^{-1}\varphi_1^{-}(z)\right)\right]\\ &-\tfrac{k_r-k_\theta}{4}\left[\tfrac{R^{-1}}{\mu_2}\left(\kappa_2 z\bar{\varphi}_2^{+}(R^2/z)+z\bar{\varphi}_2^{-}(R^2/z)\right)-\tfrac{R^{-1}}{\mu_1}\left(\kappa_1 z\bar{\varphi}_1^{-}(R^2/z)+z\bar{\varphi}_1^{+}(R^2/z)\right)\right]\\ &=-\tfrac{\sigma_0^{(1)}}{R}+\tfrac{J_0^{(1)}}{2R\mu_1}\begin{pmatrix}-\mathrm{iIm}\left\{\kappa_1 z^{-1}\varphi_1^{+}(z)-\kappa_1\varphi_1'^{+}(z)+\kappa_1 z\varphi_1''^{+}(z)+z^{-1}\varphi_1^{-}(z)-\varphi_1'^{-}(z)+z\varphi_1''^{-}(z)\right\}\\ +\kappa_1 z^{-1}\varphi_1^{+}(z)-\kappa_1\varphi_1'^{+}(z)+z^{-1}\varphi_1^{-}(z)-\varphi_1'^{-}(z)-\mathrm{Re}\left\{\kappa_1 z^{-1}\varphi_1^{+}(z)+z^{-1}\varphi_1^{-}(z)\right\}\end{pmatrix},\end{aligned}\quad |z|=R, \tag{12}$$

$$
\begin{aligned}
&\varphi_2^{'+}(z)-\varphi_2^{'-}(z)+\tfrac{k_r+k_\theta}{4}\left[\tfrac{R}{\mu_2}\left(\kappa_2 z^{-1}\varphi_2^-(z)+z^{-1}\varphi_2^+(z)\right)-\tfrac{R}{\mu_1}\left(\kappa_1 z^{-1}\varphi_1^+(z)+z^{-1}\varphi_1^-(z)\right)\right]\\
&+\tfrac{k_r-k_\theta}{4}\left[\tfrac{R^{-1}}{\mu_2}\left(\kappa_2 z\bar{\varphi}_2^+(R^2/z)+z\bar{\varphi}_2^-(R^2/z)\right)-\tfrac{R^{-1}}{\mu_1}\left(\kappa_1 z\bar{\varphi}_1^-(R^2/z)+z\bar{\varphi}_1^+(R^2/z)\right)\right] \qquad |z|=R,\\
&=-\tfrac{\sigma_0^{(2)}}{R}+\tfrac{J_0^{(2)}}{2R\mu_2}\begin{pmatrix}-\mathrm{iIm}\left\{\kappa_2 z^{-1}\varphi_2^-(z)-\kappa_2\varphi_2^{'-}(z)+\kappa_2 z\varphi_2^{''-}(z)+z^{-1}\varphi_2^+(z)-\varphi_2^{'+}(z)+z\varphi_2^{''+}(z)\right\}\\ +\kappa_2 z^{-1}\varphi_2^-(z)-\kappa_2\varphi_2^{'-}(z)+z^{-1}\varphi_2^+(z)-\varphi_2^{'+}(z)-\mathrm{Re}\left\{\kappa_2 z^{-1}\varphi_2^-(z)+z^{-1}\varphi_2^+(z)\right\}\end{pmatrix},
\end{aligned}
\tag{13}
$$

where the superscripts '+' and '−' denote limiting values as we approach the interface L from either the inside or outside, respectively.

The two analytic functions $\varphi_1(z)$, $\varphi_2(z)$ and their analytic continuations can be written in terms of the following convergent series:

$$
\begin{aligned}
\varphi_1(z)&=\begin{cases}\sum_{n=0}^{+\infty}X_nR^{-n}z^n, & |z|<R,\\ -\bar{X}_1R^{-1}z+\sum_{n=0}^{+\infty}Y_nR^nz^{-n}, & |z|>R,\end{cases}\\
\varphi_2(z)&=\begin{cases}-A\ln\frac{z-R^2/\xi}{z}+\frac{R^2(R^2-\xi^2)}{\xi^3}\frac{\bar{A}}{z-R^2/\xi}+\sum_{n=0}^{+\infty}B_nR^{-n}z^n, & |z|<R,\\ A\ln(z-\xi)+\sum_{n=0}^{+\infty}A_nR^nz^{-n}, & |z|>R,\end{cases}
\end{aligned}
\tag{14}
$$

where X_n, Y_n, A_n, B_n, $n=0,1,2,\ldots,+\infty$ are unknown complex coefficients to be determined and

$$
A=\frac{\mu_2(b_2-\mathrm{i}b_1)}{\pi(\kappa_2+1)}. \tag{15}
$$

Substituting Eq. (14) into the boundary conditions in Eqs. (12) and (13), and equating coefficients of like-powers of $z=R\mathrm{e}^{\mathrm{i}\theta}$, we finally arrive at the following sets of linear algebraic equations

$$
\begin{aligned}
&\left[2+\rho(\kappa_1-1)+\chi(\kappa_1+1)+\gamma_1(\kappa_1-1)\right]X_1+\left[2+\rho(\kappa_1-1)-\chi(1+\kappa_1)+\gamma_1(\kappa_1-1)\right]\bar{X}_1\\
&\quad-\Gamma(\rho+\chi)B_1-\Gamma(\rho-\chi)\bar{B}_1=-4R\delta_1\mu_1+\Gamma\kappa_2(\rho+\chi)E_1+\Gamma\kappa_2(\rho-\chi)\bar{E}_1,\\
&\left[\rho(1-\kappa_1)-\chi(1+\kappa_1)\right]X_1+\left[\rho(1-\kappa_1)+\chi(1+\kappa_1)\right]\bar{X}_1\\
&\quad+\left[2+\Gamma(\rho+\chi)+\gamma_2\right]B_1+\left[\Gamma(\rho-\chi)+\gamma_2\right]\bar{B}_1\\
&\quad=-4R\delta_2\mu_2+\left[2-\Gamma\kappa_2(\rho+\chi)-\gamma_2\kappa_2\right]E_1-\left[\Gamma\kappa_2(\rho-\chi)+\gamma_2\kappa_2\right]\bar{E}_1,
\end{aligned}
\tag{16}
$$

$$
\begin{aligned}
&(1+\kappa_1\gamma_1)X_2+\frac{\rho\chi}{\rho-\chi}\left[\Gamma(\kappa_2\bar{A}_0+\kappa_2\bar{E}_0+\bar{B}_0)-(\kappa_1\bar{X}_0+\bar{Y}_0)\right]=0,\\
&(1+\gamma_2)B_2-\frac{\rho\chi}{\rho-\chi}\left[\Gamma(\kappa_2\bar{A}_0+\kappa_2\bar{E}_0+\bar{B}_0)-(\kappa_1\bar{X}_0+\bar{Y}_0)\right]=(1-\kappa_2\gamma_2)E_2,
\end{aligned}
$$

$$
\Gamma(\kappa_2E_2+B_2)-\kappa_1X_2=-\frac{\rho+\chi}{\rho-\chi}\left[\Gamma(\kappa_2\bar{A}_0+\kappa_2\bar{E}_0+\bar{B}_0)-(\kappa_1\bar{X}_0+\bar{Y}_0)\right], \tag{17}
$$

$$
\begin{aligned}
&\left[2n+\kappa_1(\rho+\chi)+n^2\kappa_1\gamma_1\right]X_n+\left[\rho-\chi-n(n-2)\gamma_1\right]\bar{Y}_{n-2}-\Gamma(\rho+\chi)B_n-\kappa_2\Gamma(\rho-\chi)\bar{A}_{n-2}\\
&\quad=\Gamma\kappa_2(\rho+\chi)E_n+\Gamma(\rho-\chi)\bar{F}_{n-2},\\
&\kappa_1\left[\rho-\chi-\gamma_1n(n-2)\right]X_n+\left[2(n-2)+\rho+\chi+\gamma_1(n-2)^2\right]\bar{Y}_{n-2}-\Gamma(\rho-\chi)B_n-\Gamma\kappa_2(\rho+\chi)\bar{A}_{n-2}\\
&\quad=\Gamma\kappa_2(\rho-\chi)E_n+\Gamma(\rho+\chi)\bar{F}_{n-2},\\
&\quad-\kappa_1(\rho+\chi)X_n-(\rho-\chi)\bar{Y}_{n-2}+\left[2n+\Gamma(\rho+\chi)+\gamma_2n^2\right]B_n+\kappa_2\left[\Gamma(\rho-\chi)-\gamma_2n(n-2)\right]\bar{A}_{n-2}\\
&\quad=\left[2n-\kappa_2\Gamma(\rho+\chi)-n^2\kappa_2\gamma_2\right]E_n+\left[\gamma_2n(n-2)-\Gamma(\rho-\chi)\right]\bar{F}_{n-2},\\
&\quad-\kappa_1(\rho-\chi)X_n-(\rho+\chi)\bar{Y}_{n-2}+\left[\Gamma(\rho-\chi)-n(n-2)\gamma_2\right]B_n\\
&\quad+\left[2(n-2)+\kappa_2\Gamma(\rho+\chi)+\kappa_2\gamma_2(n-2)^2\right]\bar{A}_{n-2}\\
&\quad=\kappa_2\left[\gamma_2n(n-2)-\Gamma(\rho-\chi)\right]E_n+\left[2(n-2)-\Gamma(\rho+\chi)-\gamma_2(n-2)^2\right]\bar{F}_{n-2},\\
&\quad n=3,4,\ldots,+\infty,
\end{aligned}
\tag{18}
$$

where the dimensionless parameters ρ, χ, γ_1, γ_2, δ_1, δ_2 and Γ are defined by

$$
\rho=\frac{Rk_r}{2\mu_1},\ \chi=\frac{Rk_\theta}{2\mu_1},\ \gamma_1=\frac{J_0^{(1)}}{2R\mu_1},\ \gamma_2=\frac{J_0^{(2)}}{2R\mu_2},\ \delta_1=\frac{\sigma_0^{(1)}}{2R\mu_1},\ \delta_2=\frac{\sigma_0^{(2)}}{2R\mu_2},\ \Gamma=\frac{\mu_1}{\mu_2}, \tag{19}
$$

and the loading parameters E_0, E_n, F_n, $n = 1, 2, \ldots, +\infty$ by

$$E_0 = A\ln(-\xi),\ E_n = -\frac{A}{n}\left(\frac{R}{\xi}\right)^n,\ F_n = \left(\frac{A}{n} - \bar{A}\right)\left(\frac{R}{\xi}\right)^n + \bar{A}\left(\frac{R}{\xi}\right)^{n+2},\quad n = 1, 2, \ldots, +\infty. \tag{20}$$

It is clear from the definitions in Eq. (19) that the four size-dependent parameters γ_1, γ_2, δ_1 and δ_2 arise from surface elasticities and that the two size-dependent parameters ρ and χ arise from the spring-type imperfect interface. The two coefficients X_1 and B_1 can then be uniquely determined by solving Eq. (16), leading to

$$\begin{aligned}
X_1 &= \frac{\Gamma\rho E_1'(\kappa_2+1) - 2R\delta_1\mu_1(1+\Gamma\rho+\gamma_2) - 2R\rho\delta_2\mu_2\Gamma}{(1+\Gamma\rho+\gamma_2)\left[2+(\rho+\gamma_1)(\kappa_1-1)\right] - \rho^2\Gamma(\kappa_1-1)} + \mathrm{i}\frac{\Gamma(\kappa_2+1)}{\kappa_1+1}E_1'',\\
B_1 &= \frac{\rho(\kappa_1-1)(\rho\Gamma\kappa_2 E_1' - 2R\delta_1\mu_1) + \left[2+(\rho+\gamma_1)(\kappa_1-1)\right]\left[(1-\gamma_2\kappa_2-\rho\Gamma\kappa_2)E_1' - 2R\delta_2\mu_2\right]}{(1+\Gamma\rho+\gamma_2)\left[2+(\rho+\gamma_1)(\kappa_1-1)\right] - \rho^2\Gamma(\kappa_1-1)} + \mathrm{i}E_1'',
\end{aligned} \tag{21}$$

where E_1' and E_1'' are, respectively, the real and imaginary parts of E_1. Interestingly, the imaginary parts of X_1 and B_1 are independent of b_2 and the existence of the mixed-type interface. In addition, the imaginary part of X_1 is also independent of the elastic properties of the matrix, while that of B_1 is independent of the elastic properties of the inhomogeneity.

The three coefficients X_2, B_2 and $\kappa_1 X_0 + Y_0 - \Gamma(\kappa_2 A_0 + B_0)$ can be uniquely determined as follows by solving Eq. (17)

$$\begin{aligned}
X_2 &= \frac{E_2\rho\chi\Gamma(\kappa_2+1)}{(\rho+\chi)(1+\kappa_1\gamma_1)(1+\gamma_2) + \rho\chi\left[\Gamma+\kappa_1(1+\Gamma\gamma_1+\gamma_2)\right]},\\
B_2 &= \frac{E_2\left\{(\rho+\chi)(1+\kappa_1\gamma_1)(1-\kappa_2\gamma_2) + \rho\chi\left[\kappa_1-\kappa_2\Gamma-\kappa_1\kappa_2(\Gamma\gamma_1+\gamma_2)\right]\right\}}{(\rho+\chi)(1+\kappa_1\gamma_1)(1+\gamma_2) + \rho\chi\left[\Gamma+\kappa_1(1+\Gamma\gamma_1+\gamma_2)\right]},\\
\kappa_1 X_0 + Y_0 - \Gamma(\kappa_2 A_0 + B_0) &= \frac{\bar{E}_2\Gamma(\rho-\chi)(\kappa_2+1)(1+\kappa_1\gamma_1)}{(\rho+\chi)(1+\kappa_1\gamma_1)(1+\gamma_2) + \rho\chi\left[\Gamma+\kappa_1(1+\Gamma\gamma_1+\gamma_2)\right]} + \Gamma\kappa_2 E_0.
\end{aligned} \tag{22}$$

The four coefficients X_0, Y_0, A_0 and B_0 are constrained by Eq. $(22)_3$. Setting $X_0 = B_0 = 0$ and $A_0 = -\kappa_2 E_0$, the left coefficient Y_0 can be uniquely determined from Eq. $(22)_3$ as

$$Y_0 = \frac{\bar{E}_2\Gamma(\rho-\chi)(\kappa_2+1)(1+\kappa_1\gamma_1)}{(\rho+\chi)(1+\kappa_1\gamma_1)(1+\gamma_2) + \rho\chi\left[\Gamma+\kappa_1(1+\Gamma\gamma_1+\gamma_2)\right]}. \tag{23}$$

The coefficients X_n, Y_{n-2}, B_n, A_{n-2}, $n = 3, 4, \ldots, +\infty$ are then uniquely determined by solving Eq. (18):

$$\begin{bmatrix} \kappa_1 X_n \\ \bar{Y}_{n-2} \\ \Gamma B_n \\ \Gamma\kappa_2\bar{A}_{n-2} \end{bmatrix} = -\Gamma\begin{bmatrix} 0 \\ 0 \\ \kappa_2 E_n \\ \bar{F}_{n-2} \end{bmatrix} + \frac{2(\kappa_2+1)}{\kappa_2}\mathbf{Q}_n^{-1}\begin{bmatrix} 0 \\ 0 \\ n\kappa_2 E_n \\ (n-2)\bar{F}_{n-2} \end{bmatrix},\quad n = 3, 4, \ldots, +\infty, \tag{24}$$

where

$$\begin{aligned}
\mathbf{Q}_n = &\begin{bmatrix} \rho+\chi & \rho-\chi & -(\rho+\chi) & \chi-\rho \\ \rho-\chi & \rho+\chi & \chi-\rho & -(\rho+\chi) \\ -(\rho+\chi) & \chi-\rho & \rho+\chi & \rho-\chi \\ \chi-\rho & -(\rho+\chi) & \rho-\chi & \rho+\chi \end{bmatrix}\\
&+\begin{bmatrix} \frac{2n}{\kappa_1}+\gamma_1 n^2 & -\gamma_1 n(n-2) & 0 & 0 \\ -\gamma_1 n(n-2) & 2(n-2)+\gamma_1(n-2)^2 & 0 & 0 \\ 0 & 0 & \frac{2n+\gamma_2 n^2}{\Gamma} & -\frac{\gamma_2 n(n-2)}{\Gamma} \\ 0 & 0 & -\frac{\gamma_2 n(n-2)}{\Gamma} & \frac{2(n-2)}{\Gamma\kappa_2}+\frac{\gamma_2(n-2)^2}{\Gamma} \end{bmatrix}.
\end{aligned} \tag{25}$$

It can be shown in a relatively straightforward manner that $\mathbf{Q}_n$ is a positive definite real symmetric matrix. From Eq. (24), we can see that to determine the unknown coefficients it is sufficient to find the inverse of the 4×4 matrices $\mathbf{Q}_n$, $n = 3, 4, \ldots, +\infty$.

All of the coefficients in the expressions for $\varphi_1(z)$, $\varphi_2(z)$ and their analytic continuations have now been completely determined. The two original analytic functions $\psi_1(z)$ defined in the inhomogeneity and $\psi_2(z)$ defined in the matrix can also be conveniently obtained from Eqs. (11) and (14) as

$$\begin{aligned}
\psi_1(z) &= -\sum_{n=0}^{+\infty}\left[\bar{Y}_n + (n+2)X_{n+2}\right]R^{-n}z^n, \ |z| < R;\\
\psi_2(z) &= \bar{A}\ln(z-\xi) - \frac{\xi A}{z-\xi} - \left[\bar{A}\ln(-\xi) + \frac{A(\xi^2-R^2)}{\xi^2} + \bar{B}_0\right]\\
&\quad + \left(\frac{R}{\xi}A - \bar{B}_1\right)Rz^{-1} + \sum_{n=2}^{+\infty}\left[(n-2)A_{n-2} - \bar{B}_n\right]R^n z^{-n}, \quad |z| > R.
\end{aligned} \tag{26}$$

By substituting the analytic functions obtained into Eq. (2), we arrive at the stress field in the composite. It is clear from the above analysis that the induced stress field in the composite depends on the six size-dependent parameters ρ, χ, γ_1, γ_2, δ_1 and δ_2.

In particular, the average mean stress within the inhomogeneity and the rigid body rotation at the center of the circular inhomogeneity can be given quite simply by

$$< \sigma_{11} + \sigma_{22} > = -\frac{4\mu_1\left[\frac{\rho b_2}{\pi\xi} + 2\delta_1(1+\Gamma\rho+\gamma_2) + 2\rho\delta_2\right]}{(1+\Gamma\rho+\gamma_2)\left[2+(\rho+\gamma_1)(\kappa_1-1)\right] - \rho^2\Gamma(\kappa_1-1)}, \tag{27}$$

$$\varpi_{21} = \frac{1}{2}(u_{2,1} - u_{1,2}) = \frac{b_1}{2\pi\xi}, \quad \text{at } z = 0, \tag{28}$$

where <*> denotes the average. From Eq. (27), we can see that the sign of the average mean stress is simply opposite to that of the sum of the three terms in the square brackets in the numerator. Interestingly, the rigid body rotation at the center of the inhomogeneity in Eq. (28) is independent of the elastic properties of the composite, the imperfection of the interface and the component b_2 of the Burgers vector.

4 Image force on the edge dislocation

Using the Peach–Koehler formula [3], we can derive the image force acting on the edge dislocation. We will discuss two cases in detail: (1) The Burgers vector is normal to the interface with $b_1 \neq 0$ and $b_2 = 0$; (2) the Burgers vector is directed tangentially to the interface with $b_2 \neq 0$ and $b_1 = 0$.

4.1 The case $b_1 \neq 0, b_2 = 0$

The image force acting on the gliding dislocation can be given explicitly by

$$\begin{aligned}
F^* &= \frac{\pi R(\kappa_2+1)}{\mu_2 b_1^2}F_1 = -\frac{(\rho+\chi)(1+\kappa_1\gamma_1)(1-\kappa_2\gamma_2) + \rho\chi\left[\kappa_1 - \kappa_2\Gamma - \kappa_1\kappa_2(\Gamma\gamma_1+\gamma_2)\right]}{(\rho+\chi)(1+\kappa_1\gamma_1)(1+\gamma_2) + \rho\chi\left[\Gamma + \kappa_1(1+\Gamma\gamma_1+\gamma_2)\right]}\eta^5\\
&\quad + \sum_{n=3}^{+\infty}\eta^{2n-3}\left\{\kappa_2^{-1}(n-1)^2(1-2\eta^2) + \eta^4\left[\kappa_2 + \kappa_2^{-1}n(n-2)\right]\right\}\\
&\quad + \frac{2(\kappa_2+1)}{\Gamma\kappa_2}\sum_{n=3}^{+\infty}\eta^{2n-3}\left[0,\ 0,\ -n\eta^2,\ \kappa_2^{-1}(n-2)(n\eta^2-n+1)\right]\mathbf{Q}_n^{-1}\begin{bmatrix}0\\0\\ \kappa_2\eta^2\\ n-1-(n-2)\eta^2\end{bmatrix},\\
F_2 &= 0,
\end{aligned} \tag{29}$$

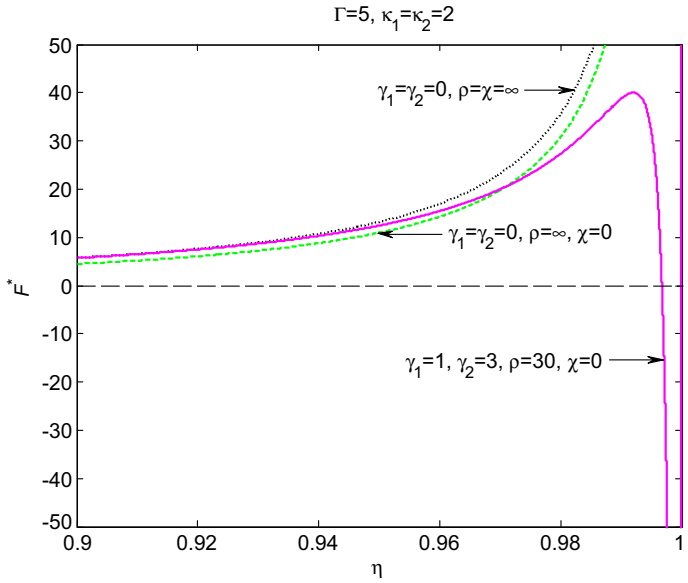

Fig. 2 Normalized image force F^* on a gliding dislocation for different values of the parameters γ_1, γ_2, ρ and χ with $\Gamma = 5, \kappa_1 = \kappa_2 = 2$

where F_1 and F_2 are, respectively, the image force components along the x_1- and x_2-directions and $\eta = R/\xi, -1 < \eta < 1$. It is seen from the above expression that the normalized image force F^* depends on the four size-dependent parameters γ_1, γ_2, ρ and χ. In other words, the normalized image force is also size dependent. It is also clear from the above expression that F^* is an odd function of η. It has been verified numerically (using MATLAB) that: (1) when choosing $\gamma_1 = \gamma_2 = 0$ and $\rho, \chi \to \infty$, Eq. (29) recovers Eq. (7.8) in [3] in the case of a perfect interface; (2) when choosing $\gamma_1 = \gamma_2 = \chi = 0$ and $\rho \to \infty$, Eq. (29) recovers Eq. (15) in [4] for a sliding interface. These results verify numerically, to a certain extent, the correctness of the solution obtained. We illustrate in Fig. 2 the normalized image force for different values of the parameters γ_1, γ_2, ρ and χ with $\Gamma = 5, \kappa_1 = \kappa_2 = 2$. The set of parameters $\gamma_1 = \gamma_2 = 0, \rho = \chi = \infty$ corresponds to a perfect interface [3], while the set $\gamma_1 = \gamma_2 = 0, \rho = \infty, \chi = 0$ describes the sliding interface [4]. From Fig. 2, we can see that the gliding dislocation is repelled from the inhomogeneity when the interface is assumed to be perfect or sliding; there exist inner stable and outer unstable equilibrium positions for the gliding dislocation (recall that $\eta = R/\xi$) when $\gamma_1 = 1, \gamma_2 = 3, \rho = 30, \chi = 0$. This fact implies that the mixed-type imperfect interface will exert a significant influence on the stability of the dislocation.

When the dislocation is located far from the inhomogeneity, the asymptotic expression for the image force can be obtained from Eq. (29) as

$$F^* = \frac{4\eta^3}{\kappa_2}\left[1 - \frac{(\kappa_2+1)\begin{pmatrix} 3(2+3\gamma_2)\left[2+\gamma_1(3\kappa_1+1)\right] \\ +\rho\left[6+2\kappa_1+2\Gamma+\gamma_1(\Gamma+16\kappa_1+3\Gamma\kappa_1)+3\gamma_2(3+\kappa_1)+24\kappa_1\gamma_1\gamma_2\right] \\ +\chi\left[6+2\kappa_1+2\Gamma+\gamma_1(\Gamma+4\kappa_1+3\Gamma\kappa_1)+3\gamma_2(3+\kappa_1)+6\kappa_1\gamma_1\gamma_2\right] \\ +2\rho\chi\left[2(\Gamma+\kappa_1)+3\kappa_1(\Gamma\gamma_1+\gamma_2)\right] \end{pmatrix}}{\begin{pmatrix} 3\left[2+\gamma_1(3\kappa_1+1)\right]\left[2+\gamma_2(\kappa_2+3)\right] \\ +\rho\begin{bmatrix}\gamma_1\left[\Gamma+(16+3\Gamma)\kappa_1+3\Gamma\kappa_2+9\Gamma\kappa_1\kappa_2\right]+\gamma_2\left[9+3\kappa_1+(3+16\Gamma)\kappa_2+\kappa_1\kappa_2\right] \\ +8\gamma_1\gamma_2\left[3\kappa_1+\Gamma\kappa_2+(1+3\Gamma)\kappa_1\kappa_2\right]+2(3+\Gamma+\kappa_1+3\Gamma\kappa_2)\end{bmatrix} \\ +\chi\begin{bmatrix}\gamma_1\left[\Gamma+(4+3\Gamma)\kappa_1+3\Gamma\kappa_2+9\Gamma\kappa_1\kappa_2\right]+\gamma_2\left[9+3\kappa_1+(3+4\Gamma)\kappa_2+\kappa_1\kappa_2\right] \\ +2\gamma_1\gamma_2\left[3\kappa_1+\Gamma\kappa_2+(1+3\Gamma)\kappa_1\kappa_2\right]+2(3+\Gamma+\kappa_1+3\Gamma\kappa_2)\end{bmatrix} \\ +2\rho\chi\left[2(\Gamma+\kappa_1)(\Gamma\kappa_2+1)+(\Gamma\gamma_1+\gamma_2)\left[3\kappa_1(\Gamma\kappa_2+1)+\kappa_2(\Gamma+\kappa_1)\right]\right] \end{pmatrix}}\right] + O(\eta^5),\ \eta \to 0. \tag{30}$$

Below, we present several typical examples to illustrate the solution and simultaneously verify its correctness.

- $\rho, \chi \to \infty$

In this case, Eq. (30) reduces to

$$F^* = \frac{4\eta^3\left[2(\Gamma+\kappa_1)(\Gamma-1)+(\Gamma\gamma_1+\gamma_2)(3\kappa_1\Gamma+\Gamma-2\kappa_1)\right]}{2(\Gamma+\kappa_1)(\Gamma\kappa_2+1)+(\Gamma\gamma_1+\gamma_2)\left[3\kappa_1(\Gamma\kappa_2+1)+\kappa_2(\Gamma+\kappa_1)\right]}, \tag{31}$$

which indicates that $\Gamma\gamma_1+\gamma_2 = (J_0^{(1)}+J_0^{(2)})/(2R\mu_2)$ can now be taken whole. If we further assume that $\gamma_1=\gamma_2=0$, Eq. (31) becomes

$$F^* = \frac{4\eta^3(\Gamma-1)}{\Gamma\kappa_2+1}, \tag{32}$$

which is just Eq. (7.13) in [3] for a perfect interface.

- $\gamma_1=\gamma_2=0$

In this case, the surface elasticities are absent. Consequently, Eq. (30) reduces to

$$F^* = \frac{4\eta^3\left[-6+(\rho+\chi)(2\Gamma-3-\kappa_1)+2\rho\chi(\Gamma-1)(\Gamma+\kappa_1)\right]}{6+(\rho+\chi)(3+\Gamma+\kappa_1+3\Gamma\kappa_2)+2\rho\chi(\Gamma+\kappa_1)(\Gamma\kappa_2+1)}. \tag{33}$$

If we further assume that $\chi=0$ and $\rho\to\infty$, Eq. (33) becomes

$$F^* = \frac{4\eta^3(2\Gamma-3-\kappa_1)}{3+\Gamma+\kappa_1+3\Gamma\kappa_2}, \tag{34}$$

which is just Eq. (19) in [4] for a sliding interface.

- $\rho=\chi=0$

In this case, Eq. (30) becomes

$$F^* = \frac{8\eta^3(\gamma_2-\kappa_2)}{\kappa_2\left[2+\gamma_2(\kappa_2+3)\right]}, \tag{35}$$

which is independent of the elastic properties of the inhomogeneity. If we further assume that $\gamma_2=0$, Eq. (35) becomes

$$F^* = -4\eta^3, \tag{36}$$

which is just the result of a gliding dislocation located far from a traction-free hole. Equation (36) can also be obtained by setting $\Gamma=0$ in Eqs. (32) or (34).

4.2 $b_2\neq 0, b_1=0$

The image force acting on the climbing dislocation can be given explicitly by

$$\begin{aligned}
F_* = \frac{\pi R(\kappa_2+1)}{\mu_2 b_2^2}F_1 = &-\frac{2\pi R(\kappa_2+1)}{b_2}\frac{\rho(\kappa_1-1)\delta_1\Gamma+\left[2+(\rho+\gamma_1)(\kappa_1-1)\right]\delta_2}{(1+\Gamma\rho+\gamma_2)\left[2+(\rho+\gamma_1)(\kappa_1-1)\right]-\rho^2\Gamma(\kappa_1-1)}\eta^2\\
&-\frac{\rho^2\Gamma(\kappa_1-1)(\kappa_2-1)+\left[2+(\rho+\gamma_1)(\kappa_1-1)\right]\left[2+(1-\kappa_2)(\Gamma\rho+\gamma_2)\right]}{(1+\Gamma\rho+\gamma_2)\left[2+(\rho+\gamma_1)(\kappa_1-1)\right]-\rho^2\Gamma(\kappa_1-1)}\eta^3\\
&-\frac{(\rho+\chi)(1+\kappa_1\gamma_1)(1-\kappa_2\gamma_2)+\rho\chi\left[\kappa_1-\kappa_2\Gamma-\kappa_1\kappa_2(\Gamma\gamma_1+\gamma_2)\right]}{(\rho+\chi)(1+\kappa_1\gamma_1)(1+\gamma_2)+\rho\chi\left[\Gamma+\kappa_1(1+\Gamma\gamma_1+\gamma_2)\right]}\eta^5\\
&+\sum_{n=3}^{+\infty}\eta^{2n-3}\left\{\kappa_2^{-1}(n-3)^2-2\eta^2\kappa_2^{-1}(n-1)(n-3)+\eta^4\left[\kappa_2+\kappa_2^{-1}n(n-2)\right]\right\}\\
&+\frac{2(\kappa_2+1)}{\Gamma\kappa_2}\sum_{n=3}^{+\infty}\eta^{2n-3}\left[0,\,0,\,n\eta^2,\,\kappa_2^{-1}(n-2)(n-3-n\eta^2)\right]\mathbf{Q}_n^{-1}\begin{bmatrix}0\\0\\-\kappa_2\eta^2\\(n-2)\eta^2-n+3\end{bmatrix}.
\end{aligned} \tag{37}$$

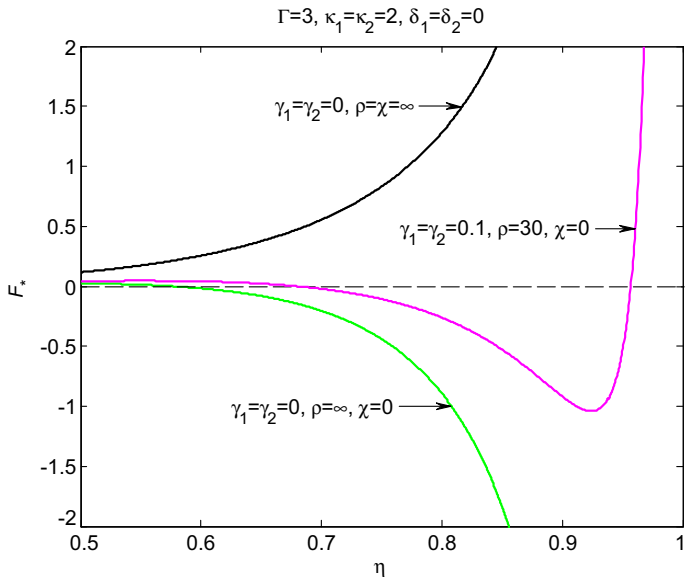

Fig. 3 Normalized image force F_* on a climbing dislocation for different values of the parameters γ_1, γ_2, ρ and χ with $\Gamma = 3$, $\kappa_1 = \kappa_2 = 2$ and $\delta_1 = \delta_2 = 0$

It is clear from the above expression that the normalized image force F_* depends on all six size-dependent parameters $\gamma_1, \gamma_2, \delta_1, \delta_2, \rho$ and χ. The existence of residual surface tensions means that F_* in Eq. (37) is no longer an odd function of η. It has been verified numerically (using MATLAB) that: (1) when choosing $\gamma_1 = \gamma_2 = \delta_1 = \delta_2 = 0$ and $\rho, \chi \to \infty$, Eq. (37) recovers Eq. (7.9) in [3] for a perfect interface; (2) when choosing $\gamma_1 = \gamma_2 = \delta_1 = \delta_2 = \chi = 0$ and $\rho \to \infty$, Eq. (37) recovers Eq. (16) in [4] for a sliding interface. Thus, the correctness of the solution has also been verified numerically. Figure 3 shows the normalized image force on a climbing dislocation for different values of the parameters γ_1, γ_2, ρ and χ with $\Gamma = 3, \kappa_1 = \kappa_2 = 2$ and $\delta_1 = \delta_2 = 0$. It is observed from Fig. 3 that the climbing dislocation is repelled from the inhomogeneity when the interface is perfect with $\gamma_1 = \gamma_2 = 0$, $\rho = \chi = \infty$; there is an unstable equilibrium position for the climbing dislocation when the interface is sliding freely with $\gamma_1 = \gamma_2 = 0$, $\rho = \infty$, $\chi = 0$; and there exist an inner stable equilibrium position and an outer unstable equilibrium position for the climbing dislocation when $\gamma_1 = \gamma_2 = 0.1$, $\rho = 30$, $\chi = 0$. The results in Figs. 2 and 3 indicate that it is possible to find multiple equilibrium positions for an edge dislocation interacting with a circular inhomogeneity with a mixed-type imperfect interface.

When the dislocation is located far from the inhomogeneity, the asymptotic expression for the image force can be extracted from Eq. (37) as

$$F_1 = -\frac{2\mu_2 b_2 \left\{\rho(\kappa_1-1)\delta_1\Gamma + \left[2+(\rho+\gamma_1)(\kappa_1-1)\right]\delta_2\right\}}{(1+\Gamma\rho+\gamma_2)\left[2+(\rho+\gamma_1)(\kappa_1-1)\right]-\rho^2\Gamma(\kappa_1-1)}\eta^2$$
$$-\frac{\mu_2 b_2^2}{\pi R(\kappa_2+1)}\frac{\rho^2\Gamma(\kappa_1-1)(\kappa_2-1)+\left[2+(\rho+\gamma_1)(\kappa_1-1)\right]\left[2+(1-\kappa_2)(\Gamma\rho+\gamma_2)\right]}{(1+\Gamma\rho+\gamma_2)\left[2+(\rho+\gamma_1)(\kappa_1-1)\right]-\rho^2\Gamma(\kappa_1-1)}\eta^3+O(\eta^5),$$
$$\eta \to 0, \tag{38}$$

which is independent of χ. The existence of residual surface tensions means that the magnitude of the image force on a climbing dislocation decays slower than that on a gliding dislocation as the dislocation moves away from the inhomogeneity. It is seen from Eq. (38) that the sign of F_1 is simply opposite to that of b_2 when the climbing dislocation is very far from the inhomogeneity. Below, several examples are presented to illustrate the solution serving also to verify the correctness of the solution.

- $\rho \to \infty$

In this case, Eq. (38) reduces to

$$F_1 = -\frac{2\mu_2 b_2(\kappa_1-1)(\delta_1\Gamma+\delta_2)}{2\Gamma+(\kappa_1-1)(\Gamma\gamma_1+\gamma_2+1)}\eta^2 - \frac{\mu_2 b_2^2}{\pi R(\kappa_2+1)}\frac{2(\kappa_1-1)-2\Gamma(\kappa_2-1)-(\Gamma\gamma_1+\gamma_2)(\kappa_1-1)(\kappa_2-1)}{2\Gamma+(\kappa_1-1)(\Gamma\gamma_1+\gamma_2+1)}\eta^3, \tag{39}$$

which also indicates that both $\Gamma\gamma_1+\gamma_2=(J_0^{(1)}+J_0^{(2)})/(2R\mu_2)$ and $\Gamma\delta_1+\delta_2=(\sigma_0^{(1)}+\sigma_0^{(2)})/(2R\mu_2)$ are now taken as whole. If we further assume that $\gamma_1=\gamma_2=\delta_1=\delta_2=0$, Eq. (39) becomes

$$F_* = \frac{2\eta^3\left[\Gamma(\kappa_2-1)-(\kappa_1-1)\right]}{2\Gamma+\kappa_1-1}, \tag{40}$$

which is just Eq. (7.14) in [3] for a perfect interface and Eq. (20) in [4] for a sliding interface. Clearly, Eq. (40) is valid for any value of χ.

- $\gamma_1=\gamma_2=\delta_1=\delta_2=0$

Now the surface elasticities are absent. In this case, Eq. (38) reduces to

$$F_* = -\frac{4+2\rho\left[\kappa_1-1-\Gamma(\kappa_2-1)\right]}{2+\rho(2\Gamma+\kappa_1-1)}\eta^3. \tag{41}$$

- $\rho=0$

In this case, Eq. (38) reduces to

$$F_1 = -\frac{2\mu_2 b_2\delta_2}{1+\gamma_2}\eta^2 - \frac{\mu_2 b_2^2}{\pi R(\kappa_2+1)}\frac{2+\gamma_2(1-\kappa_2)}{1+\gamma_2}\eta^3, \tag{42}$$

which is independent of the elastic properties of the inhomogeneity. If we further assume that $\gamma_2=\delta_2=0$, Eq. (42) becomes

$$F_* = -2\eta^3, \tag{43}$$

which is just the result of a climbing dislocation located far from a traction-free hole. Equation (43) can also be obtained by setting $\Gamma=0$ in Eqs. (40) or (41).

5 Conclusions

In this work, we have derived a rigorous solution to the problem of an edge dislocation interacting with a circular elastic inhomogeneity with a mixed-type imperfect interface. The mixed-type imperfect interface is introduced to reflect the complicated and more realistic scenario in which a soft interface represented by the spring model is bounded by two stiff interfaces arising from Gurtin–Murdoch surface elasticities. The boundary conditions on the mixed-type interface are concisely expressed in terms of $\varphi_1(z)$, $\varphi_2(z)$ and their analytic continuations. All of the complex coefficients appearing in each of these four analytic functions are obtained in a quasi-decoupled manner: X_1 and B_1 are determined by solving the two coupled linear algebraic equations in Eq. (16); X_2, B_2 and $\kappa_1 X_0+Y_0-\Gamma(\kappa_2 A_0+B_0)$ are determined by solving the three coupled linear algebraic equations in Eq. (17); and X_n, Y_{n-2}, B_n and A_{n-2} for a certain value of $n(\geq 3)$ can be determined by solving the four coupled linear algebraic equations in Eq. (18). The stress field and the image force acting on the edge dislocation can then be conveniently derived from the obtained analytic functions. Analytic expressions for the image force on gliding and climbing dislocations are presented. It is observed that in general the normalized image force depends on six size-dependent parameters γ_1, γ_2, δ_1, δ_2, ρ and χ, the first four of which result from surface elasticities and the latter two from the linear spring model. The solution to the problem of an edge dislocation inside a circular inhomogeneity with a mixed-type imperfect interface can be derived quite similarly.

Acknowledgements The authors are indebted to two reviewers whose comments and suggestions have greatly improved the manuscript. This work is supported by the National Natural Science Foundation of China (Grant No: 11272121) and through a Discovery Grant from the Natural Sciences and Engineering Research Council of Canada (Grant # RGPIN 155112).

References

1. Benveniste, Y., Miloh, T.: Imperfect soft and stiff interfaces in two-dimensional elasticity. Mech. Mater. **33**, 309–323 (2001)
2. Chen, T., Dvorak, G.J., Yu, C.C.: Size-dependent elastic properties of unidirectional nano-composites with interface stresses. Acta Mech. **188**, 39–54 (2007)
3. Dundurs, J.: Elastic interaction of dislocations with inhomogeneities. In: Mura, T. (ed.) Mathematical Theory of Dislocations, pp. 70–115. American Society of Mechanical Engineers, New York (1969)
4. Dundurs, J., Gangadharan, A.C.: Edge dislocation near an inclusion with a slipping interface. J. Mech. Phys. Solids **17**, 459–471 (1969)
5. Dundurs, J., Mura, T.: Interaction between an edge dislocation and a circular inclusion. J. Mech. Phys. Solids **12**, 177–189 (1964)
6. Dundurs, J., Sendeckyj, G.P.: Edge dislocation inside a circular inclusion. J. Mech. Phys. Solids **13**, 141–147 (1965)
7. Fan, H., Wang, G.F.: Screw dislocation interacting with imperfect interface. Mech. Mater. **35**, 943–953 (2003)
8. Fang, Q.H., Liu, Y.W.: Size-dependent elastic interaction of a screw dislocation with a circular nano-inhomogeneity incorporating interface stress. Script. Mater. **2006**(55), 99–102 (2006)
9. Gurtin, M.E., Murdoch, A.: A continuum theory of elastic material surfaces. Arch. Ration. Mech. Anal. **57**, 291–323 (1975)
10. Gurtin, M.E., Murdoch, A.I.: Surface stress in solids. Int. J. Solids Struct. **14**, 431–440 (1978)
11. Gurtin, M.E., Weissmuller, J., Larche, F.: A general theory of curved deformable interface in solids at equilibrium. Philos. Mag. A **78**, 1093–1109 (1998)
12. Luo, H.A., Chen, Y.: An edge dislocation in a three-phase composite cylinder model. ASME J. Appl. Mech. **58**, 75–86 (1991)
13. Luo, J., Xiao, Z.M.: Analysis of a screw dislocation interacting with an elliptical nano inhomogeneity. Int. J. Eng. Sci. **47**, 883–893 (2009)
14. Muskhelishvili, N.I.: Some Basic Problems of the Mathematical Theory of Elasticity. P. Noordhoff Ltd., Groningen (1953)
15. Ru, C.Q.: Simple geometrical explanation of Gurtin-Murdoch model of surface elasticity with clarification of its related versions. Sci. China Phys. Mech. Astron. **53**, 536–544 (2010)
16. Ru, C.Q., Schiavone, P.: A circular inclusion with circumferentially inhomogeneous interface in anti-plane shear. Proc. R. Soc. Lond. A **453**, 2551–2572 (1997)
17. Sharma, P., Ganti, S.: Size-dependent Eshelby's tensor for embedded nano-inclusions incorporating surface/interface energies. ASME J. Appl. Mech. **71**, 663–671 (2004)
18. Ting, T.C.T.: Anisotropic Elasticity-Theory and Applications. Oxford University Press, New York (1996)
19. Wang, X.: Interaction between an edge dislocation and a circular inclusion with an inhomogeneously imperfect interface. Mech. Res. Commun. **33**, 17–25 (2006)
20. Wang, X., Schiavone, P.: Interaction of a screw dislocation with a nano-sized, arbitrary shaped inhomogeneity with interface stresses under anti-plane deformations. Proc. R. Soc. Lond. A 470, No. 20140313 (2014). doi:10.1098/rspa.2014.0313
21. Wang, X., Schiavone, P.: A circular inhomogeneity with a mixed-type imperfect interface in anti-plane shear (under review) (2016)
22. Wang, X., Schiavone, P.: A circular inhomogeneity with a mixed-type imperfect interface under in-plane deformations. Int. J. Mech. Mater. Des. (2016). doi:10.1007/s10999-016-9345-2
23. Wang, X., Shen, Y.P.: An edge dislocation in a three-phase composite cylinder model with a sliding interface. ASME J. Appl. Mech. **69**, 527–538 (2002)
24. Xiao, Z.M., Chen, B.J.: A screw dislocation interacting with a coated fiber. Mech. Mater. **32**, 485–494 (2000)
25. Xiao, Z.M., Chen, B.J.: On the interaction between an edge dislocation and a coated inclusion. Int. J. Solids Struct. **38**, 2533–2548 (2001)